

Dislocation-based strength model for high energy density conditions

Damian C. Swift,* Kazem Alidoost, Ryan Austin, Thomas Lockard, Christine Wu, Sebastien Hamel, and John E. Klepeis
Lawrence Livermore National Laboratory, 7000 East Avenue, Livermore, California 94551, USA

Pedro Peralta
Department of Mechanical and Aerospace Engineering,
Arizona State University, P.O. Box 876106, Tempe, Arizona 85287, USA
(Dated: June 8, 2021; updates to October 11, 2021 – LLNL-JRNL-825656)

We derive a continuum-level plasticity model for polycrystalline materials in the high energy density regime, based on a single dislocation density and single mobility mechanism, with an evolution model for the dislocation density. The model is formulated explicitly in terms of quantities connected closely with equation of state (EOS) theory, in particular the shear modulus and Einstein temperature, which reduces the number of unconstrained parameters while increasing the range of applicability. The least constrained component is the Peierls barrier E_P , which is however accessible by atomistic simulations. We demonstrate an efficient method to estimate the variation of E_P with compression, constrained to fit a single flow stress datum. The formulation for dislocation mobility accounts for some or possibly all of the stiffening at high strain rates usually attributed to phonon drag. The configurational energy of the dislocations is accounted for explicitly, giving a self-consistent calculation of the conversion of plastic work to heat. The configurational energy is predicted to contribute to the mean pressure, and may reach several percent in the terapascal range, which may be significant when inferring scalar EOS data from dynamic loading experiments. The bulk elastic strain energy also contributes to the pressure, but appears to be much smaller. Although inherently describing the plastic relaxation of elastic strain, the model can be manipulated to estimate the flow stress as a function of mass density, temperature, and strain rate, which is convenient to compare with other models and inferences from experiment. The deduced flow stress reproduces systematic trends observed in elastic waves and instability growth experiments, and makes testable predictions of trends versus material and crystal type over a wide range of pressure and strain rate.

INTRODUCTION

Overwhelmingly most research on plastic flow has been devoted to engineering materials and simpler variants such as elemental Fe and Al, for deformation rates and temperatures occurring in typical applications, and at pressures around ambient, or between zero and those occurring in high-pressure static reservoirs, which is essentially the same. However, strength is important in a much wider range of materials and conditions. An extreme example is the crust of neutron stars [1], where fracture causing a break in the crust, leading to magnetic reconnection, has been proposed as a mechanism for giant gamma ray bursts in magnetars, which are powerful enough to disturb the Earth’s ionosphere from tens of thousands of light years [2]. At the intersection of science and engineering, are the impact of micrometeoroids on spacecraft, and experiments performed to investigate material properties at pressures into the terapascal scale during dynamic loading on a nanosecond time scales [3], which are directly relevant to the development of techniques for inertially-confined thermonuclear fusion [4]. As well as the sample materials studied, these experiments usually involve other components whose strength often affects the conditions imparted to or inferred in the sample. Simulations and interpretation of these experiments then must rely on models of strength that

have not been calibrated or validated in relevant conditions. Strength models can be deduced theoretically, but the detailed mechanisms of plastic flow are complicated, and have previously involved extensive multi-scale computational studies using electronic structure, molecular dynamics, and dislocation dynamics to calibrate a continuum-level model suitable for simulations of dynamic loading experiments [5, 6]. More usually, strength models used for such simulations are essentially empirical descriptions of the flow stress as a function of state, calibrated to much lower pressures, temperatures, and strain rates, with minor empirical or guessed modifications. One notable *ad hoc* simplification is that, in all widely-used continuum models, the heat imparted by flow against strength is assumed to be a constant fraction of the plastic work, often simply unity. In contrast, experimental measurements [7, 8] and theoretical studies [9–12] have found that the fraction may vary between 0.1 or less to ~ 1 over the course of a single loading event.

We have recently developed methods to predict several properties of matter efficiently over a wide range of states, including the equation of state (EOS) [13, 14], the asymptotic freedom of ions leading to the drop in their heat capacity from 3 to $3/2 k_B$ at high temperature [15], and also the shear modulus [16], which is the driving force behind plastic flow. We previously developed a dislocation-based crystal plasticity model for deformation at high pressures

and strain rates, formulated with the intention of requiring less computational effort to calibrate [17]. In the work reported here, we extend the concepts behind this model, informed by recent developments and experience, and combine it with our new predictions of shear modulus to produce a strength model valid potentially over the full range of normal matter, with particular interest in conditions occurring in high energy density (HED) applications such as loading induced by laser ablation.

We do not expect the model described here to be as accurate as models constructed from more detailed multi-scale studies over a more restricted range of states [5, 6]. However, the present model is significantly simpler to implement, includes some effects neglected in previous strength models, and can be applied in arbitrarily extreme conditions without further extension or calibration. Although we use a particular electronic structure method to supply properties needed to infer the strength over a wide range of states, the plasticity model is constructed to make it straightforward to substitute properties calculated using more detailed or accurate methods where available. It is preferable to use a strength model constructed using potentially inaccurate components than one constructed to be accurate under irrelevant conditions that would definitely be inaccurate out-with its range of calibration, or no model at all. This approach may also be suitable to estimate the plastic flow rate associated with twinning, as this process also fundamentally involves atoms hopping past a Peierls barrier.

DISLOCATION DYNAMICS

In contrast to our previous study [17], we focus here on plastic flow in polycrystalline aggregates, omitting some effects such as the change in resolved shear stress from finite elastic strains, and employing implicit averages over crystal orientations and slip systems. The constitutive equations can be solved in different ways, influenced by the internal structure of simulation programs in which they are implemented. As before [17], the intended method of solution is in continuum dynamics programs in which the local material state includes the elastic strain tensor e , from which the stress tensor τ is calculated using the bulk and shear moduli B and G , properties of the material state and in particular of the mass density ρ . G can be predicted from electronic structure theory, as in our recent wide-range study [16]. To calculate the response of the material during dynamic deformation, The driving force for plastic deformation is the deviatoric stress

$$\sigma \equiv \tau + Ip, \quad (1)$$

where the mean pressure $p = -\text{Tr} \tau / 3$. The deviatoric stress is related to the deviatoric strain

$$\epsilon = e - \mu I \quad : \quad \mu \equiv \text{Tr} e / 3 = \rho / \rho_0 - 1 \quad (2)$$

TABLE I: Scaling between Burgers vector and Wigner-Seitz radius, for simple crystal structures.

structure	f_v
body-centered cubic (bcc)	$\frac{1}{2} (9\pi)^{1/3}$
face-centered cubic (fcc)	$\frac{1}{\sqrt{2}} (2\pi/3)^{1/3}$
hexagonal close-packed (hcp), basal	$(2\pi/3)^{1/3}$
diamond	$\frac{1}{\sqrt{2}} (4\pi/3)^{1/3}$

via the shear modulus.

The plastic strain rate $\dot{\epsilon}_p$ acts to reduce the elastic strain, and is related to the dislocation density ρ_d and the mean speed of dislocation motion \bar{v}_d by a modified Orowan equation [6]

$$\dot{\epsilon}_p = \frac{\eta}{M} \rho_d b \bar{v}_d \quad (3)$$

where b is the magnitude of the Burgers vector, M the Taylor factor representing an effective number of active slip systems, and η a microstructure factor representing the number of dislocation types (1 for screw only, 2 for screw and edge). \bar{v}_d can be obtained from a kinetics model, giving a hopping rate Z , so $\bar{v}_d = bZ$. ρ_d is usually defined in conventional metallurgical terms as the dislocation line length per volume of material. At finite compressions, ρ_d and b scale with the mass density ρ . The constitutive equations become simpler, and more straightforward to generalize to large changes in compression, if expressed instead using the fraction of atoms on a dislocation,

$$\phi_d = \rho_d \frac{m_a}{b\rho} \quad (4)$$

where m_a is the mass of an atom. Then

$$\dot{\epsilon}_p = \frac{\eta}{M} \phi_d Z \gamma \quad : \quad \gamma \equiv \frac{6f_v^3}{\pi} \quad (5)$$

The ratio of Burgers vector to Wigner-Seitz radius, b/r_{WS} , is constant for a given crystal structure (Table I); for convenience we consider the distance from the equilibrium position to the peak of the Peierls barrier, $b/2$, as $f_v \equiv b/2r_{\text{WS}}$.

Previous dislocation-based strength models were constructed, and \bar{v}_d calculated, assuming dislocation motion was impeded by barriers to ‘forward’ motion [5, 6, 18, 19]. The resulting Arrhenius hopping probability gives a non-zero \bar{v}_d at zero applied stress, and various modifications have been employed to ensure that $\bar{v} \rightarrow 0$ as $\|\sigma\| \rightarrow 0$, including the use of an error function instead of an Arrhenius rate [18], and a minimum stress below which \bar{v}_d was set to zero [5, 6, 19]. As we pointed out previously [17], this problem is avoided by recognizing that atoms have no inherently preferred hopping direction, but the local stress field biases hops in the direction that reduces

shear stress [17], because the stress reduces the Peierls barrier in that direction and increases it in the opposite direction. The resulting hopping rate is

$$Z = Z_0 \left[\exp \left(-N \frac{E_P - E_\tau}{k_B T} \right) - \exp \left(-N \frac{E_P + E_\tau}{k_B T} \right) \right] \quad (6)$$

where Z_0 is the attempt rate, E_P the Peierls barrier, N the number of coordinated atom jumps required for the dislocation to move, T the temperature, and k_B Boltzmann's constant. E_τ is the effect of the local stress on the forward and reverse Peierls barriers, $\|\sigma\|v_{WS}f_v$. As well as being numerically-better conditioned as $\sigma \rightarrow 0$, the inclusion of reverse hopping reduces the net rate at elevated temperatures, giving similar phenomenological behavior as has been attributed to phonon damping, but without an additional explicit contribution or parameters. The barrier-lowering effect of the applied stress for forward hopping has also been considered by other researchers [20], and the effect of reverse hopping has been included in dislocation based studies of creep [21].

The Arrhenius rate itself represents the probability of an atom following a Maxwell-Boltzmann velocity distribution crossing a positive energy barrier greater than $k_B T$. If the stress is high enough for the barrier to become substantially smaller, the Arrhenius rate is incorrect; it should certainly not exceed unity. The mean dislocation speed is thus limited to $Z_0 b$ at high stresses, which may also be interpreted as a phonon drag.

At the microstructural level, stress is resolved on the specific slip systems and stress relaxation occurs by the motion of dislocations of each Burgers vector, with separate kinetics for each. The resolved shear stress and Burgers vector occur in the exponent of the rate equation Eq. 6, so in principle the response of polycrystalline material may be non-linear with respect to averaging of the resolved stress in the exponent and averaging of the plastic strain rate: a potential source of inaccuracy in predicting the flow stress. This averaging could be performed explicitly for a given crystal structure to go beyond the use of an assumed Taylor factor, and multiple contributions to the rate could be included with different Peierls barriers and effective attempt rates, to account for non-Schmid effects even in an average polycrystalline model. For now, we simply take a constant value M appropriate for the crystal structure and material.

Similarly, there are in general several barriers that affect the dislocation mobility, including the Peierls barrier for the ideal lattice, impurities such as interstitials, and intersections with dislocations of different Burgers vector. Usually one or other barrier dominates and controls the plastic strain rate, depending on the material, compression, temperature, applied stress, and microstructural state including the instantaneous dislocation density. In principle, several types of barrier could be incorporated even in a polycrystal-averaged model, potentially includ-

ing competition between multiple slip systems leading to non-Schmid effects and a varying effective Taylor factor. In the present work, we consider a single barrier and investigate its applicability over a wide range of conditions in the HED regime.

EVOLUTION OF DISLOCATION DENSITY

The model so far gives the plastic strain rate for a given dislocation density. Predictions of the rate of change of shear stress can be made given a measurement of the initial dislocation density in a material, but the dislocation density evolves as plastic flow occurs. A key theoretical insight leading to dislocation-based plasticity models has been the prediction that, at a given strain rate, the dislocation density evolves rapidly toward an equilibrium value [5], which can be estimated from large-scale dislocation dynamics simulations and parameterized as part of the strength model. Here we investigate an approach in which the equilibrium density $\hat{\phi}_d$ is an emergent property rather than a separately-calibrated definition. Ignoring the spontaneous generation of dislocations, if dislocations are sufficiently far apart and thus unable to annihilate each other, and considering dislocation loops from Frank-Read type sources, the rate of dislocation generation is proportional to the rate of dislocation motion:

$$\dot{\phi}_d = \frac{\pi \phi_d}{2 M} Z = \frac{\pi \dot{\epsilon}_p}{2 \gamma}. \quad (7)$$

For a given slip system, if dislocations of opposite Burgers vector occur in equal numbers, one contribution to their annihilation is collision as they move in opposite directions under the applied stress. In addition, dislocations of opposite sign attract each other through their mutual elastic strain fields, which decay with distance from each dislocation as Gb/r . Using the same method for predicting the hopping rate as for the applied stress,

$$Z_a = Z_0 \left[\exp \left(-N \frac{E_P - E_m}{k_B T} \right) - \exp \left(-N \frac{E_P + E_m}{k_B T} \right) \right] \quad (8)$$

where E_m is the adjustment to the Peierls barrier from the mutual interaction field of the dislocations,

$$E_m = \frac{Gv_{WS}f_v}{\bar{L}} \quad (9)$$

where \bar{L} is the mean separation between dislocations of opposite sign, in units of the Burgers vector,

$$\bar{L} = \sqrt{\frac{2M}{\phi_d}}. \quad (10)$$

The net rate of change in dislocation density is then

$$\dot{\phi}_d = \frac{\pi \phi_d}{2 M} Z \left(1 - \frac{2}{\bar{L}} \right) - \frac{2\phi_d Z_a}{\bar{L}} = \frac{\dot{\epsilon}_p \pi}{\gamma 2} \left(1 - \frac{2}{\bar{L}} \right) - \frac{2\phi_d Z_a}{\bar{L}}. \quad (11)$$

Adjustment factors may be included for each term to match more detailed modeling where available.

If the dislocation population is in equilibrium, $\dot{\phi}_d = 0$, and $\hat{\phi}_d$ can be deduced from Eq. 11, which can be solved numerically by bisection since $0 \leq \phi_d \leq 1$. Dependence on state and strain rate enters through the attraction term only. Neglecting this term,

$$\hat{\phi}_d = M/2 > 1. \quad (12)$$

This limiting case could be the result of oversimplification in the generation and collision terms, such as the use of the mean separation \bar{L} . There presumably is a limiting value of ϕ_d , ϕ_{\max} say, above which the concept of dislocations is meaningless. In practice, ϕ_d must remain well below 1, for the crystal lattice to be stable [22]. To correct for too large a ϕ_{\max} from the asymptotic limit of the generation and collision terms, we include an additional saturation term to limit ϕ_d to some chosen ϕ_{\max} :

$$\dot{\phi}_d = R_m(\phi_{\max} - \phi_d) - R_c - R_a \quad (13)$$

where R_m , R_c , and R_a are the rates from multiplication, collision, and attraction respectively, from Eq. 11.

STRAIN AND GRAIN HARDENING

Dislocation-based strength models implemented in hypoelastic form usually include a semi-empirical term to represent the increase of flow stress with plastic strain, interpreted as associated with a resulting increase in ρ_d , for instance [6] $\hat{\tau} = \zeta b G \sqrt{\rho_d}$. For our purposes it would be preferable to represent this kind of behavior consistently with the mobility of the dislocations or evolution of ϕ_d . Strain hardening could be interpreted in several related ways. When dislocations intersect and tangle, a greater bowed length of dislocation is needed to accommodate a given amount of plastic strain. In a bowed dislocation, a greater proportion of the length must overcome a barrier closer to the full E_P rather than $E_P - E_\tau$, which could be represented a hop rate Z depending on the mean free dislocation length \bar{L} . Alternatively, this effect could be represented as a reduction in ϵ_p for a given $\dot{\phi}_d$, and thus an increase in the strain energy of the dislocations e_d , i.e. $\dot{\epsilon}(\bar{L})$ or $M(\bar{L})$. An additional barrier term could be included for unpinning of tangled dislocations. However it is represented, strain hardening may also have an effect on dislocation annihilation.

As a trial model of hardening, we estimate the mean distance between dissimilar dislocation intersections as

$$\bar{L}'b \quad : \quad \bar{L}' = \sqrt{\frac{M-1}{\phi_d}}, \quad (14)$$

leading to a (further) modified Orowan equation

$$\dot{\epsilon}_p = \frac{\eta}{M} \phi_d Z \gamma f_h \quad : \quad f_h \equiv 1 - \frac{1}{\bar{L}'}. \quad (15)$$

The hardening term f_h can thus be considered equivalent to an effective M , Z , or ϕ_d . A further benefit is that we can attempt to incorporate the Hall-Petch grain size effect [23, 24] in the same spirit by including an additional contribution to \bar{L}' representing the stiffening effect of grain boundaries:

$$f_h = 1 - \sqrt{\frac{\phi_d}{M-1}} + f_{\text{HP}} \phi_g, \quad (16)$$

where ϕ_g is, in similar convention to ϕ_d , the fraction of atoms on a grain boundary. Considering the surface area to volume ratio of a grain, expressed in terms of r_{WS} ,

$$\phi_g \simeq \frac{12r_{\text{WS}}}{\lambda_g} \quad (17)$$

for equiaxed grains. f_{HP} is a geometrical factor for the distance from a point on a dislocation to the nearest grain boundary. We estimate f_{HP} to be approximately 2, though if based on the average chord of a sphere [25] it may be closer to 3. In practice we limit $f_h \geq 0$ for numerical safety.

ENERGETICS

An important unresolved question in plasticity is the relation between plastic work and heating, which can be represented by the Taylor-Quinney factor [26, 27]. The core energy of a screw dislocation amounts to around $Gb^2/2$ per length, i.e. $Gb^3/2$ per b of line. The elastic strain energy for well-separated dislocations is similar. The specific energy associated with the dislocation population is then

$$e_d \simeq G \frac{f_b^3 \phi_d}{\rho}. \quad (18)$$

At high dislocation densities, the strain fields from dislocations of opposite Burgers vector tend to cancel out, leading to a more general energy

$$e_d \simeq \frac{Gb^2}{4\pi(1-\nu)} \frac{\rho_d}{\rho} \ln \frac{1}{b\sqrt{\rho_d}} \quad (19)$$

where the Poisson ratio ν can be determined using quantities more readily available in applications at high pressure as $(3B - 2G)/(6B + 2G)$. The energy depends in detail on the dislocation type and the grain orientation with respect to the load [28]. To capture this behavior in a bounded way, preserving the core energy at high dislocation densities, we make the replacement

$$\phi_d \rightarrow \alpha \phi_d \ln \sqrt{\frac{\phi_c}{\phi_d}} \quad (20)$$

in Eq. 18, where

$$\frac{1}{\alpha} = \ln \frac{\phi_{\max}}{\phi_{\text{ref}}} \simeq 4\pi, \quad \phi_c = \phi_{\max} e^{1/\alpha}. \quad (21)$$

Potential energy stored in the dislocation population in this way reduces the energy available for plastic heating. Conversely, as dislocations annihilate, which may occur at zero total strain rate, the temperature will rise.

If the material is compressed isotropically at a constant dislocation population ϕ_d , the specific energy of the dislocations changes. Neglecting entropy effects, this change appears as a contribution to the pressure

$$p_d = \rho e_d \left(\frac{\rho}{G} \frac{\partial G}{\partial \rho} - 1 \right). \quad (22)$$

In principle, p_d could have either sign. In our atom-in-jellium predictions of $G(\rho)$ [16], the exponent of ρ was almost always greater than 1, so $p_d > 0$. In molecular dynamics simulations of plastic flow at constant pressure [29], an expansion of 0.5 to $1 r_{\text{WS}}$ per b of dislocation length has been observed [30]. Counteracting this expansion to maintain a constant mass density corresponds to a similar increase in pressure.

FINITE ELASTIC STRAIN

In continuum dynamics programs intended for high pressure simulations, the mean pressure p is assumed to depend on isotropic strain only, through the EOS, and the stress deviator σ is assumed to be traceless. We found previously using electronic structure simulations of elastic deformation [31] that this assumption is incorrect, i.e. that the mean pressure at a given mass density and temperature varies with the elastic strain deviator. We assessed the effect as probably unimportant on microsecond and longer time scales, where elastic strains in metals do not typically exceed $\sim 10^{-3}$, but noted that it may matter on shorter time scales such as are explored in laser-loading experiments, where elastic strains may reach several percent.

Thermodynamically, any contribution to mean pressure from the strain deviator should be caused by the elastic distortional energy,

$$e_e = \frac{1}{2\rho} G \|\epsilon_e\|^2. \quad (23)$$

Neglecting the temperature dependence of G , and at constant $\|\epsilon_e\|$, the contribution to mean pressure is

$$p_e = \rho e_e \left(\frac{\rho}{G} \frac{\partial G}{\partial \rho} - 1 \right). \quad (24)$$

FLOW STRESS

Although inherently describing the dependence of the plastic strain rate on the applied stress, a flow stress can be deduced from this model. The flow stress is useful

for comparison with experiment, or in simulations where it is not practical to implement the plastic strain rate as a relaxation of elastic strain. Consider a situation where the total strain rate is $\dot{\epsilon}$ at some ρ and T . The flow stress Y is the external stress needed to give $\dot{\epsilon}_p \simeq \dot{\epsilon}$. If the dislocation population is in equilibrium, $\dot{\phi}_d = 0$, and ϕ_d can be deduced from Eq. 11, which can be solved numerically by bisection since $0 \leq \phi_d \leq 1$. The shear stress $\|\sigma\| = Y$ can then be found such that

$$\frac{\eta}{M} \phi_d Z(\sigma) \gamma f_h = \dot{\epsilon}_p \quad (25)$$

i.e.

$$Y = \sqrt{\frac{3}{2}} \frac{k_B T}{v_{\text{WS}} f_v} \sinh^{-1} \left[\frac{\dot{\epsilon}_p}{2\gamma \phi_d f_h} \frac{M \exp(E_P/k_B T)}{Z_0} \right]. \quad (26)$$

At the equilibrium dislocation density, the leading term in dislocation density is roughly proportional to $\sqrt{\phi_d}$, consistent with Taylor hardening [32] and observations from molecular dynamics simulations of plasticity [28].

Eq. 26 can be used to construct an approximate model expressing for example $Y(\rho, \dot{\epsilon}_p)$ along some reference curve such as an isentrope. To estimate the flow stress away from the reference curve, i.e. at different temperatures, Eq. 26 can be differentiated with respect to temperature to obtain a softening relation

$$\left. \frac{\partial Y}{\partial T} \right|_{\rho} = \frac{Y}{T} - \frac{E_P}{v_{\text{WS}} f_v T} \frac{\xi}{\sqrt{1 + \xi^2}} \quad (27)$$

where

$$\xi \equiv \frac{\dot{\epsilon}_p}{2\gamma \phi_d f_h} \frac{M \exp(E_P/k_B T)}{Z_0} \quad (28)$$

Along an isochore, $\partial Y/\partial T$ may be positive, i.e. the material may harden rather than soften with temperature, depending on the relative magnitude of the two terms.

The flow stress Y above is not a yield stress: $\dot{\epsilon}_p > 0$ for stresses $\|\sigma\| < Y$. However, Y provides an indication of when the material responds to an externally-applied stress largely with plastic flow rather than elastic strain.

PROPERTIES FROM ELECTRONIC STRUCTURE

Z_0 can be determined from the ion-thermal contribution to the EOS. Used in conjunction with EOS constructed using atom-in-jellium theory, it is convenient to use the Einstein temperature θ_E , which is calculated by perturbation of the nucleus from its equilibrium position. The corresponding Einstein vibration frequency

$$Z_E = k_B \theta_E / h, \quad (29)$$

where h is Planck's constant. In the absence of more detailed information, the Peierls barrier can also be estimated from θ_E , assuming similarity of the shape of the

potential surface experienced by the atoms. Z_E is calculated assuming a harmonic potential, with a stiffness

$$k = m_a (2\pi Z_E)^2. \quad (30)$$

The potential surface is stiffer than harmonic along directions toward a neighboring atom, and softer along other directions. Along a Burgers vector, the force must become zero at $b/2$. We estimate E_P by extrapolating the harmonic potential at some fraction of b , equivalent to some fraction f_b $O(1)$ of r_{ws} :

$$E_P \simeq k (f_b r_{ws})^2. \quad (31)$$

Suggestively, approximately correct flow stresses are obtained with $f_b \sim 0.1 - 0.3$. This range is consistent with our generalization of the Lindemann melting law which matches melting of the one-component plasma with $f_b = 0.15$, and melting at lower pressures with similar or slightly lower values [14, 33]. This similarity suggests a somewhat different connection with melting than previous suggestions of a dislocation-mediated process [34] or critical equilibrium population of dislocations [35]. The Lindemann parameter is usually interpreted as a melting criterion involving the mean square displacement of the atoms. Our observation suggests that this mean square displacement may correspond to the kinetic energy required for atoms to hop past the Peierls barrier, and thus to an abrupt decrease in the resistance to shear stress.

The Einstein or Debye frequencies are average phonon frequencies that seem reasonable to represent a typical attempt rate for an atom to hop past a potential barrier, at least to predict systematic trends. Phonon frequencies range from zero to a value corresponding to the stiffest elastic modulus. Low frequencies represent acoustic modes in which atoms move in the same direction as their neighbors. High frequencies represent optic modes in which atoms oscillate in antiphase with their nearest neighbors. Neither leads to hopping. In the atom-in-jellium model, surrounding atoms are treated as uniform positive and negative charge densities, in which neighbors and gaps are not distinguished.

Our previous melting studies used the Debye temperature inferred from the jellium oscillation model [14, 33]. Here we use the Einstein temperature, for a more direct connection with the stiffness of the effective interatomic potential. Because of the method used to infer Debye from Einstein temperature in our previous work, $f_b = 0.15$ in the melting studies requires an additional scaling factor $\sqrt[3]{\pi/6} \simeq 0.8$ for use with the Einstein temperature. Accordingly, we consider a default value of 0.12.

EXAMPLES

The most direct predictions and comparisons of a plasticity model are the observables in a specific loading scenario. However, experimental measurements on dynamic loading have wide variations in loading history, and require an assessment of the EOS and shear modulus as well as the plastic flow, so we will report experiment-by-experiment comparisons elsewhere. For illustration here, we predict systematic trends in the plastic response of several elemental metals of different crystal structures, whose strength is of current interest in high pressure experiments. For simplicity, we ignore the effect of high-pressure phase transitions, though these can be taken into account. To construct strength models, we use our previous atom-in-jellium predictions of the EOS and shear modulus [16, 36].

Some trends are observed repeatedly in the strength of materials during deformation at high rates and elevated pressure, so far unexplained by plasticity theory. The flow stress inferred from elastic precursor waves is typically several times greater on nanosecond time scales typical of laser ablation experiments than on microsecond time scales typical of gun and high explosive experiments [37]. In contrast, the flow stress inferred from Rayleigh-Taylor strength experiments at pressures in the ~ 100 GPa range is typically a couple of times higher than predicted using the Steinberg-Guinan (SG) strength model [38].

We consider the variation of flow stress with pressure along the principal isentrope, for simplicity neglecting the temperature increase from plastic work. We adopted f_v for the appropriate crystal structure, and took a value of M typical for elements of that structure. We chose $\eta = 1$ on the basis that, for large strains, any initial population of pure edge dislocations would be swept away, leaving dislocations produced by Frank-Read sources, which are of mixed type. The sole remaining parameter is then f_b . Because of its connection to melting of the one-component plasma, we first chose $f_b = 0.12$ to give an entirely first-principles (but typically inaccurate) strength model. We also determined a value f_b to reproduce an experimental measurement of Y . This could be done by performing simulations of an experiment, such as of an elastic wave amplitude. For convenience and consistency between different materials, we instead fitted f_b to reproduce the SG value of Y_0 for each material [39–41] (Table II), using Eq. 26 and making the common assumption of a representative strain rate and zero pressure, and taking the equilibrium dislocation density $\dot{\phi}_d$. Values of the representative strain rate for experiments on millimeter to centimeter scale samples measuring the response on microsecond scales are commonly held to be $\sim 10^5 - 10^6$ /s. We determined values of f_b for different strain rates, and found that elastic wave amplitudes

TABLE II: Plasticity parameters and EOS used for isentrope.

	f_v	f_b	M	isentrope
Al	fcc	0.096261	3.64	SESAME 3717
Cu	fcc	0.123206	3.64	SESAME 3336
Ag	fcc	0.126552	3.64	LEOS 470
Ir	fcc	0.111460	3.64	LEOS 770
Pt	fcc	0.087128	3.64	LEOS 780
Au	fcc	0.099675	3.64	LEOS 790
Pb	fcc	0.192771	3.64	LEOS 820
Fe	bcc	0.150433	3.0	SNL-SESAME 2150
Ta	bcc	0.099455	3.0	LEOS 735
W	bcc	0.125096	3.0	LEOS 740
Be	hcp	0.141415	2.0	LEOS 40
Ru	hcp	0.12	2.0	LEOS 440

predicted using the SG model were reproduced closely in centimeter scale samples when calibrated using $10^6/s$, i.e. the present model and calibration process is consistent with a characteristic strain rate of $10^6/s$ for elastic precursor waves in centimeter-scale samples, and this is the normalization used for all results shown below.

Given a value of f_b , we predicted $Y(\dot{\epsilon}, p)$ taking $\{T, p\}(\rho)$ from the isentrope. Atom-in-jellium EOS are often inaccurate at pressures below a few tenths of a terapascal, so we took the principal isentropes from semi-empirical wide-range EOS libraries [42, 43], also as listed in Table II. To emphasize: the plasticity model above is defined in terms of ρ , T , ϵ_e , and ϕ_d : it does not depend explicitly on pressure, and so the choice of EOS is not an inherent part of the model. (The shear modulus and Einstein temperature should in principle be consistent with the EOS, and the Peierls barrier is also related to the EOS though less directly.)

Dislocation densities in bulk engineering materials are typically $\sim 10^8/cm^2$ i.e. $\phi_d \sim 10^{-7}$. For any reasonable value of f_b , the resulting flow stress was much larger than observed in dynamic loading experiments, indicating that ϕ_d must increase rapidly to accommodate the resulting plastic strain rate. Such increases have been inferred experimentally in studies of shaped charge jets [44], in molecular dynamics simulations [45], and in dislocation dynamics simulations [5, 6] of high-rate loading. Except for transient effects as the strain rate is varied, it has been found possible to estimate the flow stress during high-rate loading from the equilibrium dislocation density instead of considering its instantaneous evolution [46]. In the figures below, we do the same and calculate the equilibrium density $\hat{\phi}_d$ given the state and $\dot{\epsilon}_p$.

A corollary is that it may be simpler than often suspected to predict the strength of a material following a phase change. Dislocations in the original phase are likely to disappear in any diffusive phase transformation, and the dislocation population in the new phase is likely to depend on the details of crystal nucleation and growth.

However, if the dislocation density evolves rapidly toward an equilibrium value as further deformation occurs, the density on first formation may matter little for the subsequent flow stress.

Considering the sensitivity to strain rate at zero pressure (Figs 1 to 3), taking $f_b = 0.12$ predicts that the fcc metals ordered by increasing flow stress are Pb, Ag, Au, Cu, Pt, Al, Ir whereas the SG Y_0 order is Pb, Au, Pt, Al, Ag, Cu (no model for Ir). It is possible that the SG Y_0 may be higher than that of the pure element where impurities are common, such as Al, Cu, and Pb. The most striking outlier is Al, which is notable because $f_b = 0.12$ appears valid for melting [33]. For the bcc metals, the predicted order is Fe, Ta, W, in accordance with the SG Y_0 . No SG parameter set has been published for pure Fe, and the fit was performed for stainless steel. For the hcp metals considered, Be is predicted to have much lower flow stress than Ru.

For most materials starting at the lowest strain rates considered here, the flow stress is predicted to increase by roughly a factor of three per order of magnitude increase in strain rate. At sufficiently high strain rates, the sensitivity is predicted to decrease as the applied stress reduces the effective height of the Peierls barrier. This regime is reached at a lower strain rate in stronger elements, and occurs well below the theoretical maximum strength of the crystal is reached, which would be when $Y = G/2\pi$. The net effect accounts roughly for the observed difference in elastic wave amplitudes between microsecond and nanosecond scale experiments.

Analyzing the behavior in more detail (Figs 4 to 10), elements of lower Z such as Be are predicted to retain a large dependence of flow stress on strain rate to high pressures. For fcc elements of moderate to high Z , the sensitivity of flow stress to strain rate is large at low pressures but decreases at pressures above ~ 100 GPa. For bcc elements of moderate to high Z , the sensitivity of flow stress to strain rate is less than that of fcc elements at low pressure, but decreases more slowly with pressure. For Ta in particular, the flow stress at pressures of a few hundred gigapascals and a strain rate $10^7/s$ representative of Rayleigh-Taylor ripple growth experiments is close to twice the SG Y_{\max} value.[49] The flow stress of metals including Ta and Au has been estimated at pressures ~ 0.1 TPa and strain rates $10^5 - 10^6/s$, from release features in the velocity history transmitted through ramp-loaded samples [47]. This is a recent approach and the uncertainties are relatively large, but the trend and magnitude appear consistent with our predictions.

The contribution of the core and strain energy of the dislocations is predicted to be significant. At low pressures, calculated as above, it can easily exceed the pressure from the EOS. This is misleading, because we are concerned with near-uniaxial loading, and it is not possible to sustain the strain rate for long enough to build up an equilibrium population of dislocations before the

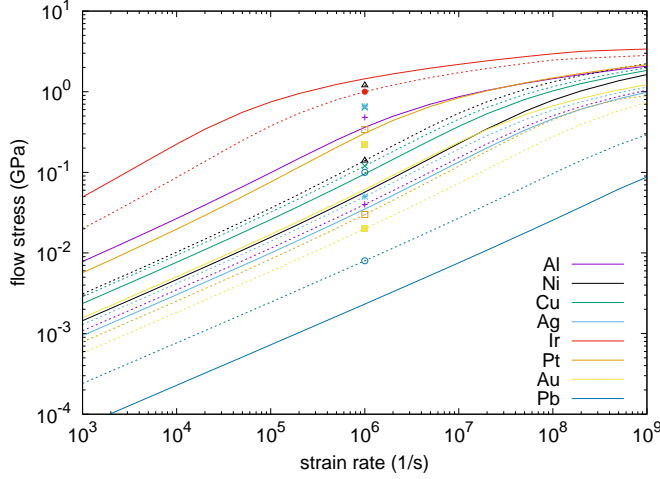


FIG. 1: Flow stress for face-centered cubic elements at zero pressure, predicted with $f_b = 0.12$ (solid) and with f_b fitted to SG Y_0 (dashed). Symbols show Y_0 and Y_{\max} where available.

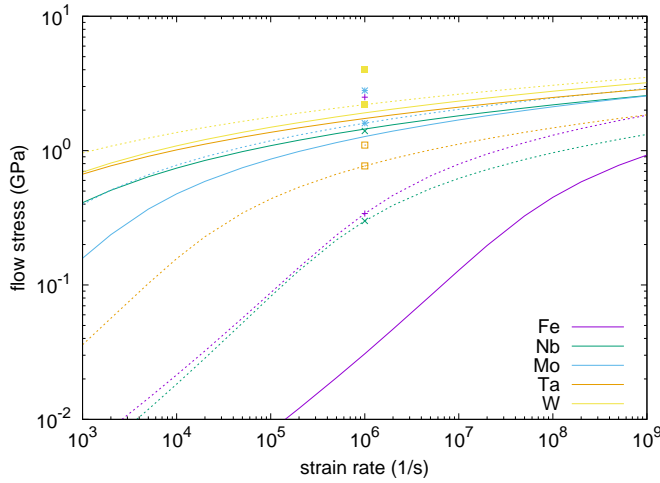


FIG. 2: Flow stress for body-centered cubic elements at zero pressure, predicted with $f_b = 0.12$ (solid) and with f_b fitted to SG Y_0 (dashed). Symbols show Y_0 and Y_{\max} where available.

pressure rises substantially. However, for pressures into the terapascal range, the dislocation pressure tends toward a few percent of the mean pressure, which may be a significant correction when interpreting dynamic loading behaviour in terms of the scalar EOS.

The sensitivity of flow stress to relevant strain rates has previously been investigated in Al and Fe [48]. The strain rate was estimated from the rate of acceleration of the rear surface of the sample, and it was concluded that Al exhibited effects of phonon drag for strain rates above $10^3/s$, whereas Fe exhibited a transition from thermal activation to phonon drag above $\sim 5 \times 10^6/s$. The reduced data exhibited significant scatter in log space, but there are some inconsistencies in the deduced flow stress, for instance the value for Al lay well above the SG

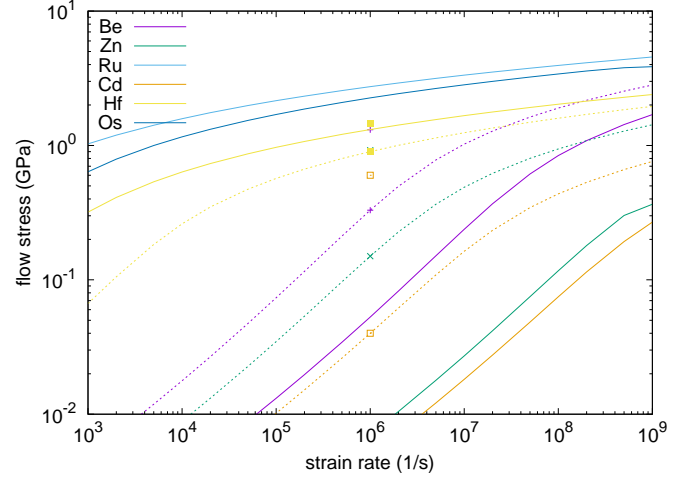


FIG. 3: Flow stress for hexagonal close-packed elements at zero pressure, predicted with $f_b = 0.12$ (solid) and with f_b fitted to SG Y_0 (dashed). Symbols show Y_0 and Y_{\max} where available.

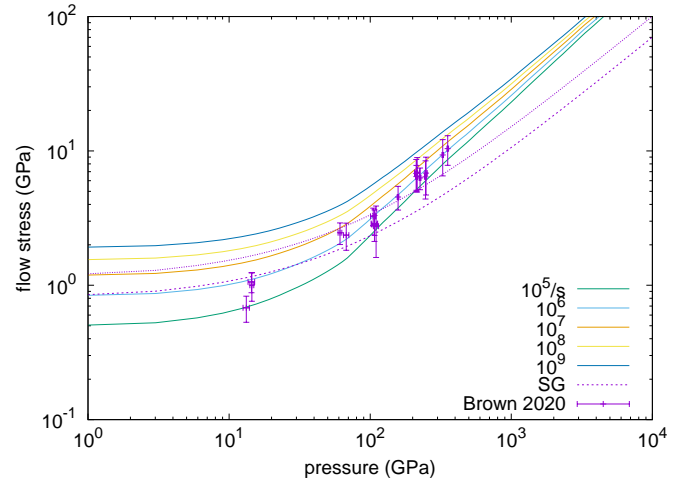


FIG. 4: Predicted variation of flow stress with pressure and strain rate along the principal isentrope of Ta, f_b fitted to SG Y_0 . Magenta lines: SG Y_0 (lower) and Y_{\max} (upper), with predicted dependence on pressure and temperature along the isentrope.

Y_0 value. Space- and time-resolved simulations of these experiments capturing the propagation and evolution of the compression wave may shed more light on the discrepancy, for example by a modified metric for strain rate and also by accounting for the evolution from initial dislocation density. For a simple comparison, we adjusted f_b to reproduce the magnitude of the fit to the reduced data at $10^6/s$ in Al and $5 \times 10^6/s$ in Fe: $f_b = 0.122261$ and 0.177440 respectively. Plotting the flow stress in linear space to highlight the stiffness of the sensitivity to strain rate, the model prediction for Al reproduces the rapid increase in flow stress with strain rate without requiring an explicit phonon drag term (Fig. 11). The prediction

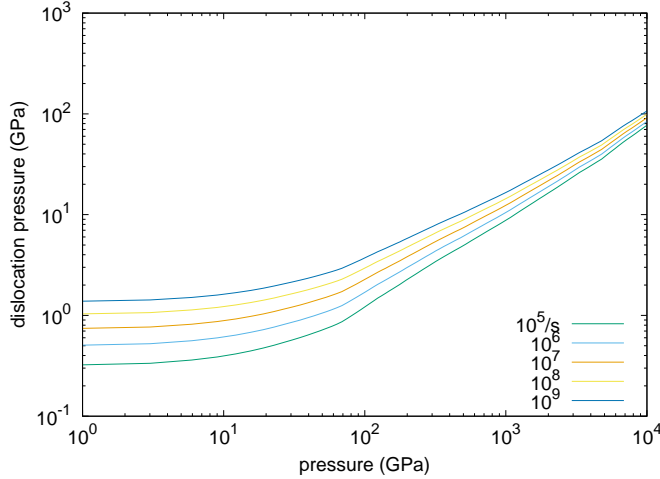


FIG. 5: Predicted variation of dislocation pressure with pressure and strain rate along the principal isentrope of Ta, f_b fitted to SG Y_0 .

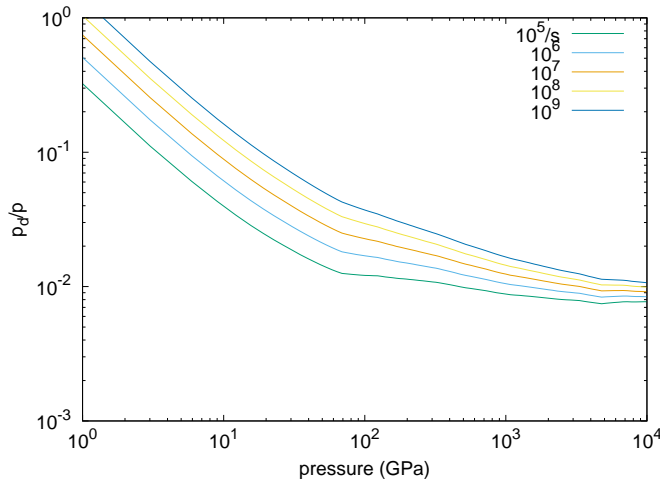


FIG. 6: Predicted ratio of dislocation pressure p_d to pressure p along the principal isentrope of Ta, f_b fitted to SG Y_0 .

for Fe did not exhibit the same degree of stiffening. As well as the same caveats about resolving the propagating waves and accounting for the evolving dislocation density, additional complexities for Fe include the impedance mismatch with the transparent window and phase transformations which occurred during the laser-driven experiments and could affect the driving stress.

CONCLUSIONS

We describe a continuum-level plasticity model for polycrystalline materials based on a single dislocation density and single mobility mechanism, with an evolution model for the dislocation density. Using the approximate but wide-ranging and computationally efficient atom-in-

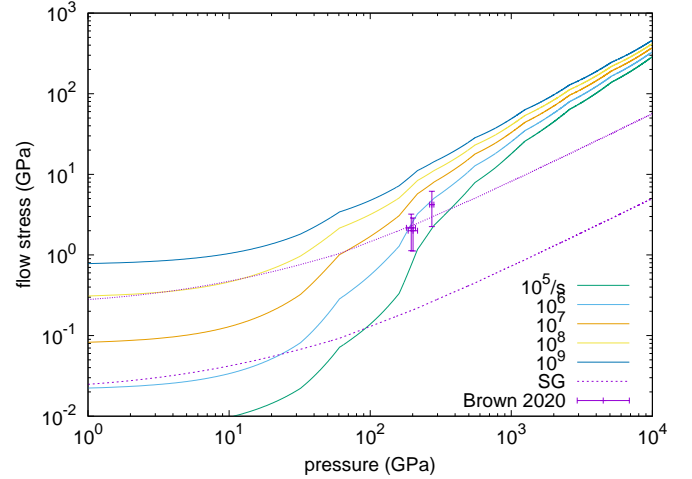


FIG. 7: Predicted variation of flow stress with pressure and strain rate along the principal isentrope of Au, f_b fitted to SG Y_0 . Magenta lines: SG Y_0 (lower) and Y_{\max} (upper), with predicted dependence on pressure and temperature along the isentrope.

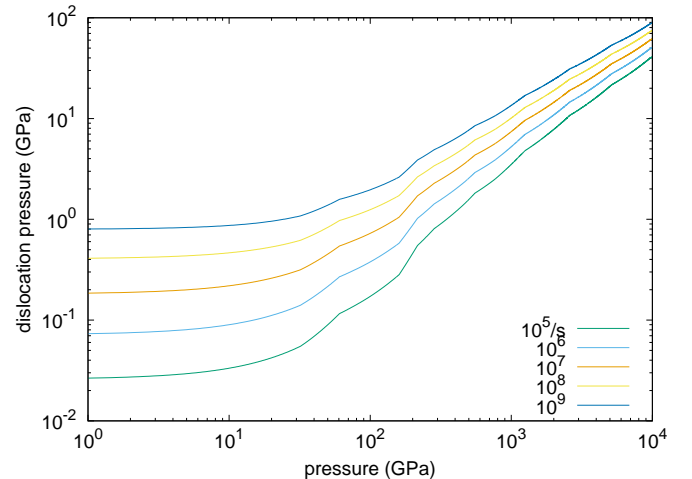


FIG. 8: Predicted variation of dislocation pressure with pressure and strain rate along the principal isentrope of Au, f_b fitted to SG Y_0 .

jellium model for the electronic structure of matter to predict the shear modulus, Einstein frequency, and systematic variation of the Peierls barrier, we deduce a credible variation of flow stress with pressure and strain rate. In this formulation, the equilibrium dislocation density is an emergent property of the model. With the dislocation density expressed per-atom rather than as a dislocation length per volume, to simplify the plasticity relations at finite compressions, its value was predicted to vary less with pressure. Interestingly, stiffening at high strain rates that is usually attributed to phonon drag may be accounted for by the form of the hopping rate.

The model is constructed to make it straightforward to

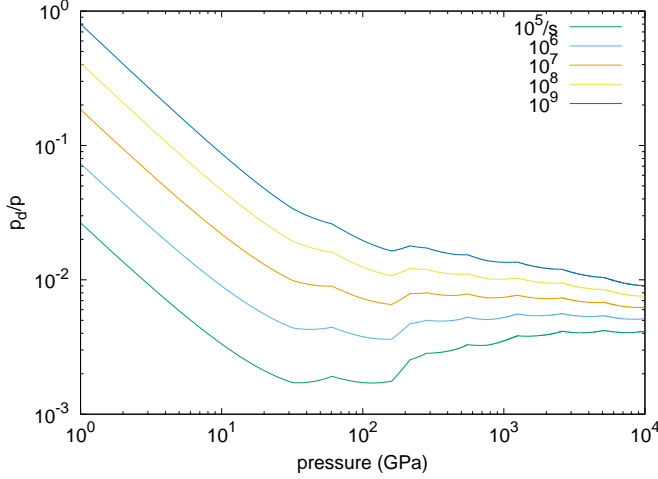


FIG. 9: Predicted ratio of dislocation pressure p_d to pressure p along the principal isentrope of Au, f_b fitted to SG Y_0 .

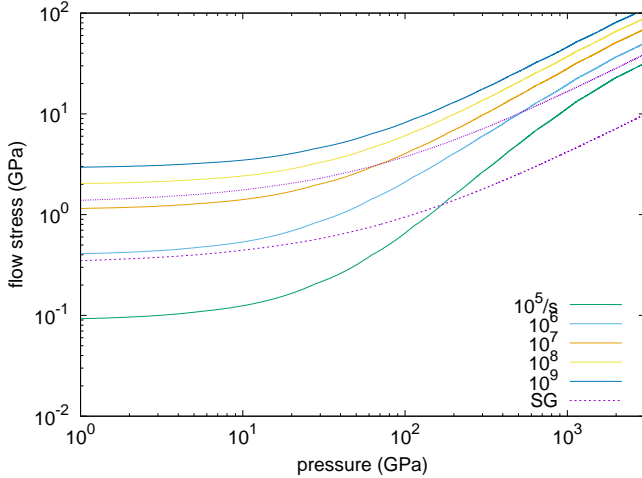


FIG. 10: Predicted variation of flow stress with pressure and strain rate along the principal isentrope of Be, f_b fitted to SG Y_0 . Magenta lines: SG Y_0 (lower) and Y_{\max} (upper), with predicted dependence on pressure and temperature along the isentrope.

substitute alternative forms for key components, such as the shear modulus, hopping attempt rate, Peierls barrier, and terms in the dislocation evolution equation, where more accurate relations are available. It may also be possible to generalize the dislocation mobility to account for several types of barrier, represented with a rheonet.

In estimating the Peierls barrier from the Einstein frequency, we find a potential link to the Lindemann melting law, which leads to a parameter-free approximate plasticity model. This approach otherwise requires a single free parameter to be determined from experiment or more detailed theory.

Accounting for the elastic energy of the dislocations gives a prediction of the plastic work appearing as heat,

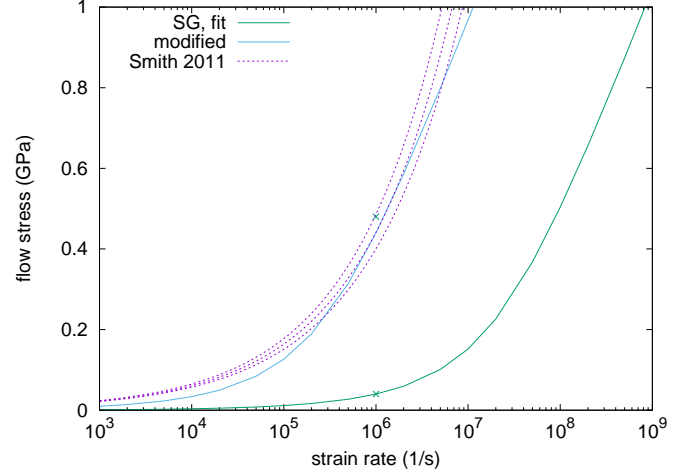


FIG. 11: Predicted variation of flow stress with pressure and strain rate along the principal isentrope of Al and as deduced from rear surface velocity measurements [48].

i.e. a dynamic, self-consistent estimate of the Taylor-Quinney factor, which has long been a poorly-constrained parameter or assumption in simulations of plastic flow. The elastic energy of the dislocations is predicted to be manifested also as a contribution to the pressure, which may reach several percent of the total pressure in ramp compression to the terapascal range, and should therefore be considered when interpreting ramp data as an isentrope or isotherm. The bulk elastic strain energy also contributes to the pressure, but is much smaller. The mean pressure is usually assumed to depend only on the scalar equation of state and not on the elasticity or strength: both of these contributions represent new physics.

The model reproduces the observation that the elastic wave amplitude for loading of samples $o(10) \mu\text{m}$ thick, on nanosecond time scales, corresponds to a flow stress a few times higher than for samples $o(10) \text{mm}$ thick, on microsecond time scales. It predicts a reduced dependence of flow stress on strain rate in higher- Z materials, particularly in the face-centered cubic structure, at pressures over ~ 100 GPa. The predictions are reasonably consistent with recent assessments of strength at high pressure from surface velocimetry data.

Acknowledgments

The authors would like to acknowledge informative conversations with Dean Preston, Vasily Bulatov, Nicolas Bertin, Jared Stimac, Sylvie Aubry, Nathan Barton, Robert Rudd, and Philip Sterne. This work was performed under the auspices of the U.S. Department of Energy under contract DE-AC52-07NA27344.

* Electronic address: dswift@llnl.gov

- [1] C.J. Horowitz and K. Kadau, *Phys. Rev. Lett.* **102**, 191102 (2009).
- [2] P. Campbell, M. Hill, R. Howe, J.F. Kielkopf, N. Lewis, J. Mandaville, A. McWilliams, W. Moos, D. Samouce, J. Winkler, G.J. Fishman, A. Price, D.L. Welch, P. Schnoor, A. Clerkin, and D. Saum, Gamma-ray Coordinates Network (GCN) Gamma Ray Burst (GRB) Observation report 2932, Am. Assoc. Variable Star Observers, aavso.org and <https://gcn.gsfc.nasa.gov> (2005).
- [3] For example, H.-S. Park, K.T. Lorenz, R.M. Cavallo, S.M. Pollaine, S.T. Prisbrey, R.E. Rudd, R.C. Becker, J.V. Bernier, and B.A. Remington, *Phys. Rev. Lett.* **104**, 135504 (2010); R. Rygg, R.F. Smith, A.E. Lazicki, D.G. Braun, D.E. Fratanduono, R.G. Kraus, J.M. McNaney, D.C. Swift, C.E. Wehrenberg, F. Coppari, M.F. Ahmed, M.A. Barrios, K.J.M. Blobaum, G.W. Collins, A.L. Cook, P. Di Nicola, E.G. Dzenitis, S. Gonzales, B.F. Heidl, M. Hohenberger, A. House, N. Izumi, D.H. Kalantar, S.F. Khan, T.R. Kohut, C. Kumar, N.D. Masters, D.N. Polsin, S.P. Regan, C.A. Smith, R.M. Vignes, M.A. Wall, J. Ward, J.S. Wark, T.L. Zorbrist, A. Arsenlis, and J.H. Eggert, *Rev. Sci. Instrum.* **91**, 043902 (2020).
- [4] J. Lindl, *Phys. Plasmas* **2**, 3933 (1995).
- [5] N.R. Barton, J.V. Bernier, R. Becker, A. Arsenlis, R. Cavallo, J. Mariani, M. Rhee, H.-S. Park, B.A. Remington, and R.T. Olson, *J. Appl. Phys.* **109**, 073501 (2011).
- [6] N.R. Barton and M.R. Rhee, *J. Appl. Phys.* **114**, 123507 (2013).
- [7] J.J. Mason, A.J. Rosakis and G. Ravichandran, *Mech. Materials* **17**, 135-145 (1994).
- [8] R. Kapoor and S. Nemat-Nasser, *Mech. Materials* **27**, 1-12 (1998).
- [9] P. Rosakis, A.J. Rosakis, G. Ravichandran, and J. Hodowany, *J. Mech. Phys. Solids* **48**, 581-607 (2000).
- [10] J. Hodowany, G. Ravichandran, A.J. Rosakis, and P. Rosakis, *Exp. Mech.* **40**, 2, 113-123 (2000).
- [11] A. Zubelewicz, *Phys. Rev. B* **77**, 214111 (2008).
- [12] A. Zubelewicz, *Sci. Rep.* **9**, 9088 (2019).
- [13] D.C. Swift, T. Lockard, M. Bethkenhagen, R.G. Kraus, L.X. Benedict, P. Sterne, M. Bethkenhagen, S. Hamel, and B.I. Bennett, *Phys. Rev. E* **99**, 063210 (2019).
- [14] D.C. Swift, T. Lockard, S. Hamel, C.J. Wu, L.X. Benedict, P.A. Sterne, and H.D. Whitley, [arXiv:2103.03371](https://arxiv.org/abs/2103.03371) (2021).
- [15] D.C. Swift, T. Lockard, M. Bethkenhagen, S. Hamel, A. Correa, L.X. Benedict, P.A. Sterne, and B.I. Bennett, *Phys. Rev. E* **101**, 053201 (2020).
- [16] D.C. Swift, T. Lockard, S. Hamel, C.J. Wu, L.X. Benedict, and P.A. Sterne, [arXiv:2105.12303](https://arxiv.org/abs/2105.12303) (2021).
- [17] D.C. Swift, E.N. Loomis, P. Peralta, and B. El-Dasher, [arXiv:0801.0271](https://arxiv.org/abs/0801.0271) (2008).
- [18] D.L. Preston, D.L. Tonks, and D.C. Wallace, *J. Appl. Phys.* **93**, 211 (2003).
- [19] R.A. Austin, *J. Appl. Phys.* **123**, 035103 (2018).
- [20] C.S. Deo, D.J. Srolovitz, W. Cai, and V.V. Bulatov, *J. Mech. Phys. Solids* **53**, 1223-1247 (2005).
- [21] F.A. Nichols, *Mater. Sci. Eng.* **8**, pp 108-120 (1971).
- [22] R.M.J. Cotterill, *Phys. Lett.* **A 60**, 61-62 (1977).
- [23] E.O. Hall, *Proc. Phys. Soc. Lond.* **64**, 9, 747-753 (1951).
- [24] N.J. Petch, *J. Iron Steel Inst. London.* **173**, 25-28 (1953).
- [25] P.A.M. Dirac, "Approximate Rate of Neutron Multiplication for a Solid of Arbitrary Shape and Uniform Density," British Report MS-D-5, Part I. (1943); in R.H. Dalitz (Ed.), "The Collected Works of P. A. M. Dirac 1924-1948," pp 1115-1128 (Oxford University Press, Oxford, 1995).
- [26] W.S. Farren and G.I. Taylor, *Proc. Roy. Soc.* **A107**, 422 (1925).
- [27] G.I. Taylor and H. Quinney, *Proc. Roy. Soc.* **A143**, 307 (1934).
- [28] N. Bertin (Lawrence Livermore National Laboratory), private communication (2021).
- [29] L.A. Zepeda-Ruiz, A. Stukowski, T. Oettel, and V.V. Bulatov, *Nature* **550**, 492 (2017).
- [30] V. Bulatov (Lawrence Livermore National Laboratory), private communication (2021).
- [31] D.C. Swift and G.J. Ackland, *Appl. Phys. Lett.* **83**, 1151 (2003).
- [32] G.I. Taylor, *Proc. Roy. Soc.* **A145**, 362 (1934).
- [33] D.C. Swift, T. Lockard, R.F. Smith, C.J. Wu, and L.X. Benedict, *Phys. Rev. Research* **2**, 023034 (2020).
- [34] F.D. Stacey and R.D. Irvine, *Aust. J. Phys.* **30**, 641-646 (1977).
- [35] L. Burakovsky, D.L. Preston, and R.R. Silbar, *Phys. Rev. B* **61**, 22, 15011 (2000).
- [36] T. Lockard et al, in preparation.
- [37] K. Alidoost et al, in preparation.
- [38] H.-S. Park, K.T. Lorenz, R.M. Cavallo, S.M. Pollaine, S.T. Prisbrey, R.E. Rudd, R.C. Becker, J.V. Bernier, and B.A. Remington, *Phys. Rev. Lett.* **104**, 135504 (2010).
- [39] M.W. Guinan and D. Steinberg, *J. Phys. Chem. Solids* **35**, 1501 (1974).
- [40] D.J. Steinberg, S.G. Cochran, and M.W. Guinan, *J. Appl. Phys.* **51** (3), 1498-1504 (1980).
- [41] D.J. Steinberg, Lawrence Livermore National Laboratory report UCRL-MA-106439 change 1 (1993).
- [42] S.P. Lyon and J.D. Johnson, Los Alamos National Laboratory report LA-UR-92-3407 (1992).
- [43] D.A. Young and E.M. Corey, *J. Appl. Phys.* **78**, 3748 (1995).
- [44] B. Goldstein (DERA Fort Halstead), private communication (1993).
- [45] S.G. Srinivasan, M.I. Baskes, and G.J. Wagner, *J. Mat. Sci.* **41**, 23, 7838-7842 (2006).
- [46] R.E. Rudd (Lawrence Livermore National Laboratory), unpublished.
- [47] J.L. Brown, J.-P. Davis, and C.T. Seagle, *J. Dyn. Behavior Mat.* **7**, 196-206 (2021).
- [48] R.F. Smith, J.H. Eggert, R.E. Rudd, D.C. Swift, C.A. Bolme, and G.W. Collins, *J. Appl. Phys.* **110**, 123515 (2011).
- [49] Rayleigh-Taylor ripple growth experiments are typically designed to give a plastic strain of a few tens of percent. At these strains, the work-hardening term in the SG strength model for Ta has reached Y_{max} .